frontiers | Frontiers in Energy Research

ORIGINAL RESEARCH
published: 01 June 2022
doi: 10.3389/fenrg.2022.878171

Raman Spectroscopy of Nascent Soot Oxidation: Structural Analysis During Heating

G. De Falco[1], S. Bocchicchio[2], M. Commodo[2], P. Minutolo[2]* and A. D'Anna[1]*

[1]Dipartimento di Ingegneria Chimica, dei Materiali e della Produzione Industriale, Università degli Studi di Napoli "Federico II", Napoli, Italy, [2]Istituto di Scienze e Tecnologie per l'Energia e la Mobilità Sostenibili, STEMS-CNR, Napoli, Italy

The effect of oxidation on nascent soot particles is investigated in this work by means of Raman spectroscopy. Three different soot particle samples are produced in a lightly sooting ethylene/air laminar premixed flame and collected at different residence times. The samples are characterized by a different size of primary particles and a different degree of aging and hence graphitization, and they are representative of the early evolution of nascent soot in flames. Oxidation of particles is induced by exposing the samples to a high temperature oxidation treatment in air over a range of temperature 25–500°C. To this aim, a programmable heating microscope stage is used. Thermo-optical transmission (TOT) measurements are used to characterize the chemical composition of pristine particles in terms of organic and elemental carbon content, also providing the pyrolytic carbon fraction of the organic carbon. The TOT results show that the organic fraction is constant for the three conditions. On the other hand, the pyrolytic carbon fraction decreases and the elemental carbon increases when moving from the sample composed of just-nucleated particles to the sample mostly made of mature soot particles. Raman spectroscopy reveals that the thermal oxidation treatment performed on the sample of just-nucleated particles, with the highest organic carbon content, results in a reduction of the amorphous carbon component. Conversely, the sample of mature soot, with the highest elemental carbon content, shows an increase in the amorphous carbon phase after oxidation, which is attributed to fragmentation or the formation of point defects by O_2 oxidation. Finally, the thermal oxidation procedure produces a strong reduction in the photoluminescence signal detected from Raman spectra.

Keywords: nascent soot, soot oxidation, Raman spectroscopy, organic carbon, elemental carbon

OPEN ACCESS

Edited by:
Lipo Wang,
Shanghai Jiao Tong University, China

Reviewed by:
Bo Jiang,
Nanjing University of Science and Technology, China
Ibukun Oluwoye,
Murdoch University, Australia

****Correspondence:***
G. De Falco
gianluigi.defalco@unina.it
P. Minutolo
patrizia.minutolo@stems.cnr.it

Specialty section:
This article was submitted to Advanced Clean Fuel Technologies, a section of the journal Frontiers in Energy Research

Received: *17 February 2022*
Accepted: *12 May 2022*
Published: *01 June 2022*

Citation:
De Falco G, Bocchicchio S, Commodo M, Minutolo P and D'Anna A (2022) Raman Spectroscopy of Nascent Soot Oxidation: Structural Analysis During Heating. Front. Energy Res. 10:878171. doi: 10.3389/fenrg.2022.878171

INTRODUCTION

The incomplete combustion of fossil and bio-derived fuels produces a large variety of carbonaceous species including particulates, namely soot particles. Soot formation in flames and combustion devices has been the object of numerous studies over the years motivated by their negative effects on the human health and on the environment (Hansen and Nazarenko, 2004; Davidson et al., 2005; Kennedy, 2007; Bond et al., 2013; Pedata et al., 2015). The formation mechanism comprises numerous phases, often overlapped, that may be summarized in some fundamental steps including particle nucleation, growth and agglomeration, in addition to carbonization and oxidation reactions (Baldelli et al., 2020; Michelsen et al., 2020; Martin et al., 2022). Each of

them is strongly dependent on the specific operative conditions of the combustion process, including fuel structure, flame temperature, pressure and type of combustion configuration, i.e., degree of premixing, turbulence, etc.

Among the abovementioned processes involved in the formation and evolution of soot in flames, oxidation is particularly relevant in consideration of mitigating the amount of carbon particulates released from a combustion process. In addition, knowing the phenomena of the soot oxidation process is also important in consideration of the currently adopted after treatment technologies implemented for the removal of the particles at the exhausts of a vehicle. These systems, indeed, require periodic cleaning/regenerative procedures by means of carbon-burn-off methods and thus by oxidizing the carbon deposits (Niessner, 2014). Finally, it is well recognized that once released in the atmosphere, the primary soot particles, i.e., combustion-generated soot, undergo significant oxidative reactions, which may also alter their water affinity tendency. Under these conditions, primary soot nanoparticles, which commonly have a hydrophobic or even a superhydrophobic character, may convert into more hydrophilic species and thus acting as water condensation nuclei eventually, with several and complex direct and indirect effects on the climate change (Decesari et al., 2002; Zuberi et al., 2005).

Numerous studies have shown that nascent soot nanoparticles present physicochemical properties significantly different from aged/mature soot or black carbon particles, for which oxidation reactivity is typically investigated (Molina et al., 2004). For instance, it was found that nascent soot particles carry significant aliphatic components (Santamaría et al., 2006; Cain et al., 2011; Minutolo et al., 2011; Schulz et al., 2019), radicals (Commodo et al., 2019; Vitiello et al., 2019) and the graphitic order typically increases with the particle residence time in flame (Kholghy et al., 2013; Apicella et al., 2015; Commodo et al., 2015; Botero et al., 2019). Hydrogen content also differ from just formed to mature/aged soot particles (Faccinetto et al., 2020), and consistently the amount of organic carbon for the nascent soot particles reduces as the residence time increases (Bocchicchio et al., 2022). It is well known that soot oxidation reactivity strongly depends on soot nanostructure (Vander Wal and Tomasek, 2004) and on the fraction of organic carbon composing the carbonaceous particles (Ess et al., 2016). One further point that may impact soot oxidation is that recently the relevance of the radical characters in some polycyclic aromatic hydrocarbons, PAHs, has been evidenced with respect to soot surface reactions. The mass growth rate of reactions involving spin-triplet polycyclic aromatic hydrocarbon may be one order of magnitude larger than that of the surface hydrogen-abstraction-carbon-addition (HACA) reaction (Zhang et al., 2015). Interesting, the radical characters in PAHs also facilitate addition of oxygen molecules (Altarawneh et al., 2020) and the inclusion of persistent π-radicals in kinetic models has recently allowed to improve the interpretation of experimental soot oxidation data (Nobili et al., 2022).

Motivated by the above considerations, the kinetic of nascent soot particle oxidation was studied through electrical mobility measurements for thee valuation of particle size distributions before and after oxidation by Camacho et al. (2015). The rate measured for the nascent soot particles was an order of magnitude larger than that predicted by the well-known Nagle Strickland-Constable (NSC) correlation (Nagle and Strickland-Constable, 1962), indicating that the surface of nascent/young soot was indeed more reactive towards oxidation than graphitized soot. Soot oxidation and fragmentation studies were also carried out experimentally by Lighty and coauthors (Echavarria et al., 2011; Echavarria et al., 2012; Ghiassi et al., 2016a; Ghiassi et al., 2016b; Sirignano et al., 2016) in a two-stage burner, where soot was produced in a first-stage premixed burner and then oxidized in a second stage, under fuel-lean and slightly-rich conditions. The authors suggested a strong fragmentation of the soot aggregates due to oxygen penetration through the breakup of the bridges connecting the particles (Echavarria et al., 2011; Echavarria et al., 2012; Ghiassi et al., 2016a; Ghiassi et al., 2016b; Sirignano et al., 2016). Similar results have been numerically obtained by Sirignano et al. (2013). More recently, Sediako et al. (2017) used for the first time an environmental high-resolution transmission electron microscope for *in-situ* soot oxidation measurements. The oxidation of mature soot was shown to mainly occur through surface reactions with ionized oxygen species, leading to a progressive decrease of the particle diameter and to a weakening of the bridges between the particles, thus ultimately causing the aggregate to fragment. On the other side, less mature primary particles, collected at lower residence times in the flame, were shown to exhibit internal oxidation in addition to the surface reactions with the disordered carbon easily burned away (Sediako et al., 2017).

Raman spectroscopy has become an increasingly common experimental method to characterize carbonaceous nanoparticles providing structural and chemical information of soot under a variety of conditions and environments (Sadezky et al., 2005; Herdman et al., 2011; Seong and Boehman 2013; Minutolo et al., 2014; Bonpua et al., 2019; Commodo et al., 2020; Salamanca et al., 2020). In this study, we aim at investigating the effect of nascent soot oxidation by Raman spectroscopy. Soot particles with different sizes and maturity have been collected form a laminar premixed flame of ethylene/air by sampling at different residence times. Soot oxidation experiments have been carried out by means of a temperature-controlled stage operated with air while the effect of the oxidative treatment has been investigated, *in situ*, by Raman spectroscopy.

EXPERIMENTAL SECTION

Flame and Sampling Condition

Nascent soot particles were collected from a laminar premixed flat flame burning an ethylene-air mixture. The cold gas velocity was set at 9.8 cm/s and carbon to oxygen (C/O) atomic ratio was fixed at 0.67, (equivalence ratio Φ = 2.01). Electronic flow controllers (Bronkhorst High-Tech BV) and a McKenna burner (Holthuis & Associates) were used to assure long-term flame stability and a highly repeatability for particle formation. The laminar premixed flat flame configuration furnishes a combustion environment in which the reaction time, and thus

particle dynamic, only depends on the height above the burner, so that particles of different size, chemical structure and morphology can be selected by sampling at a specific height. Soot particles were extracted from the flame centerline using a dilution horizontal tubular probe with a small orifice, i.e., 600 microns in diameter, located on the bottom side, as described in several earlier works (Commodo et al., 2015; Commodo et al., 2019; Schulz et al., 2019; Vitiello et al., 2019; Bocchicchio et al., 2022). Flame temperature profiles measured with and without probe are reported elsewhere (Commodo et al., 2015). This sampling procedure allows the quenching of chemical reactions throughout the sampling line.

Soot samples were collected at 8, 10 and 14 mm burner-to-probe distance (Z), by changing the probe position with respect to the burner surface. From now on, we will refer to these samples as Z8, Z10 and Z14, respectively. The selected locations correspond to the earlier stages of soot formation, i.e., nucleation and initial growth. The sampled soot ranges from very small particles with an average size of the order of 3.5 nm for the Z8 sample, to 8.1 nm for Z10, and 18.5 nm for the Z14 soot sample. Information on particle size distribution measurements at these flame locations, obtained by on-line scanning mobility particle sizing, are reported elsewhere (Commodo et al., 2015; Commodo et al., 2019; Schulz et al., 2019; Vitiello et al., 2019; De Falco et al., 2021).

A stainless-steel aerosol filter holder (Merk–Millipore Mod. XX5004700) containing a quartz filter (Whatman QMA–grade, 47 mm) was positioned on-line downstream of the dilution tubular probe for soot collection. Gas temperature at the filter location was about 80°C. The particle collection lasted several hours in order to collect enough material on the filter for the analysis.

Soot Oxidation and Raman Spectroscopy

The *in-situ* temperature-dependent Raman spectroscopy analysis was performed on a ~1 cm^2 piece of the soot loaded quartz filter, directly positioned inside the programmable heating microscope stage (Mod. Linkam HFS600E-PB4, Linkam Scientific Instruments, United Kingdom) without further manipulations. Soot was heated in air up to 500°C. The heating was programmed with a 15°C/min ramp and a holding time of 10 min at each temperature step to perform the Raman spectroscopy measurements. After reaching the maximum temperature of 500°C, the microscope stage was left to cool down to ambient temperature and Raman spectra were again taken as the temperature of 250°C and ambient temperature were reached, to verify soot modification upon temperature/oxidation treatment. For each temperature step, a few minutes were waited to allow the sample to stabilize thermally before starting the spectroscopic analysis.

Raman spectroscopy measurements were performed on the samples positioned in the heating stage under the Raman microscope (Mod. XploRA, Horiba, Japan) equipped with a long working distance 50X objective (NA0.5 Olympus, Germany), a Nd:YAG laser (λ = 532 nm, 12 mW maximum laser power at the sample) and a 200 μm pinhole for confocal photons collection. The diffraction grating had 1,200 groves/mm and the central position was 1,600 cm^{-1}. System calibration was performed against the Stokes Raman signal of pure silicon at 520 cm^{-1}. The power of the excitation laser beam was attenuated to 1% to avoid structural changes of the sample due to thermal decomposition when using an accumulation-exposure time of 5 cycles of 30 s each. Five spots were randomly selected over the soot loaded quartz filter to verify the homogeneity of the sample and finally averaged to obtain a statistically relevant Raman spectrum. The standard deviation was of the order of few percent.

Using the Raman microscope, laser-induced emission spectra were also measured on a wide range. Since soot particles at the earlier stages of formation, i.e., nucleation and initial growth excited by visible light emit broad fluorescence spectra (De Falco et al., 2020) a diffraction grating with 600 groves/mm was used and the central wavelength was set to 650 nm to measure the fluorescence spectra on the spectral range 550–750 nm.

Thermo-Optical Transmission Analysis

A rectangular punch (1.5 × 1 cm) was used to remove the central portion of the filter for thermo-optical-transmission analysis using a Lab OC-EC Aerosol Analyzer from Sunset Laboratory Inc. with a Detection Limit DL = 0.2 μg/cm^2. The sampling time was set in order to collect a mass of particles greater than the DL, by assuming a uniform deposition on the filter surface.

Thermo-optical transmission (TOT) measurements allow to measure the Total Carbon (TC) of the particles collected on the filters, as well as to separate the fractions of Organic Carbon (OC) and Elemental Carbon (EC). OC is defined as the carbon containing species that do not absorb visible light and are released off of the heated filter in an inert bath gas (He) without oxygen. EC, or Black Carbon (BC), is defined as the visible-absorbing carbon that requires a high temperature oxidizing environment to evolve off of the filter (Birch and Cary, 1996). A NIOSH-like protocol was used, consisting of 4 temperature steps (310°C, 475°C, 615°C, 870°C) in a completely oxygen-free helium atmosphere, followed by cooling to 550°C, and a second heating series in helium/oxygen mixture of 8% oxygen with temperature steps at 625°C, 700°C, 775°C, 850°C and 870°C. For each flame condition, repeated measurements were done to reduce uncertainties to less than 6%.

In TOT measurements, while OC evolves from the filter part of the sample becomes more absorbing. This effect occurring during the first inert, oxygen-free, heating phase has been well documented by many researchers (Yu et al., 2002; Chow et al., 2004; Giannoni et al., 2016) and is explained by some fraction of OC that may char and is pyrolytically converted to a carbon form that absorbs visible light. Such pyrolized OC fraction requires an oxidizing atmosphere to evolve off the filter, and thus would be counted erroneously as EC if all the carbon evolving from the filter during the oxidizing atmosphere phase was attributed to EC, overestimating this component. In TOT, this pyrolytic conversion or charring process is continuously monitored by measuring the transmission of a laser (λ = 678 nm) through the filter. As a result of charring, the light transmission decreases from the initial value. During the second heating phase in the He/O_2 mixture, both the original EC as well as the pyrolytically converted OC (PC) are counted as they evolve from the filter causing a concomitant monotonic increase in the ligth

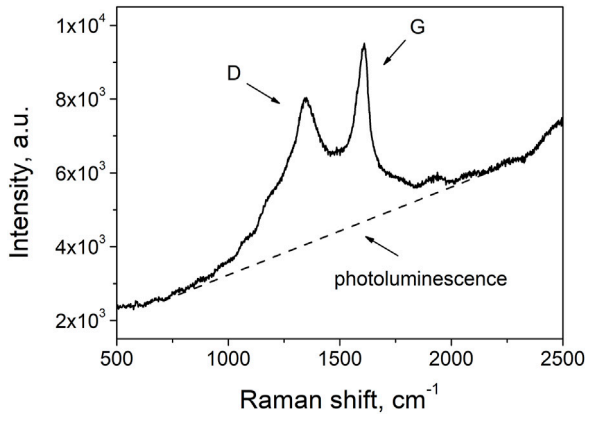

FIGURE 1 | First-order Raman spectrum of flame soot. Note: the spectrum refers to the Z8 sample at ambient temperature.

transmission until all carbon from the filter is removed and counted. The protocol allows to separately quantify these two components setting the "OC-EC split" at the point in the second heating phase in the oxidative bath gas where the laser transmission value is equal to the original value measured prior to heating the sample. Carbon evolving after this line is counted as native or original EC, and carbon evolving prior to this split is counted as PC. The total OC (OC_{tot}) is equal to the sum of PC and OC. This char correction procedure relies on the assumptions that PC has similar optical properties to EC, and that PC evolves at a lower temperature prior to EC in the protocol (Chow et al., 2004).

RESULTS AND DISCUSSION

Raman and Photoluminescence Spectra

A typical first-order Raman spectrum of nascent soot particles is reported in **Figure 1**. The main features derives from the two major peaks known as D (defect) and G (graphite) bands whose maximum are located at approximatively 1,350 cm^{-1} and 1,600 cm^{-1} respectively. These two Raman peaks are typical of any amorphous/disordered carbon-based material and reflect the highly defective character characteristic of the soot nanoparticle, particularly at the very early stages of the formation process. Indeed, the presence of defects in the sp^2 aromatic network allows the activation of the Raman D mode at ~1,350 cm^{-1}, which is prohibited in the perfect hexagonal lattice (Castiglioni et al., 2001). Conversely, the G band, at ~1,600 cm^{-1}, due to every sp^2 bond, is mostly insensitive to the presence of defects, thus only presenting small changes in width and position of the maximum as a function of the different carbon structures. The relative Raman intensity of the D and G bands is, therefore, a measure of the degree of order in an amorphous carbon sample and it is often correlated to the size of the aromatic domains whiting the carbon network. Details on the physical origin of these two Raman modes can be found elsewhere (Ferrari and Robertson, 2004).

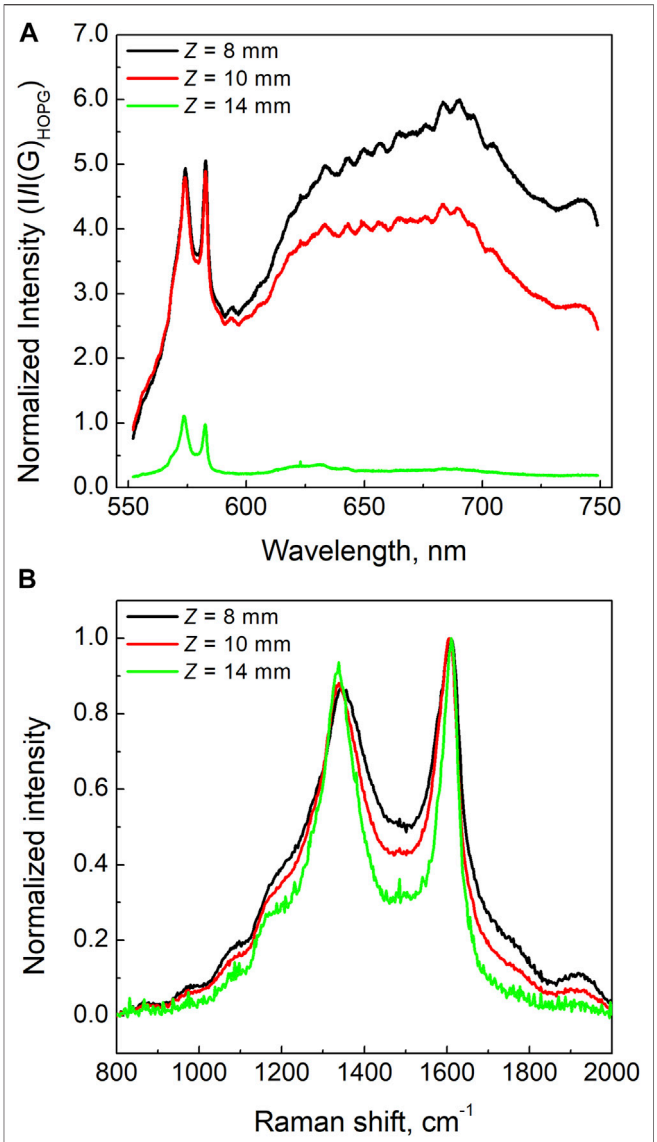

FIGURE 2 | (A) Photoluminescence spectra of the soot samples normalized by the intensity of the G band of HOPG; **(B)** Raman spectra of three different soot samples background subtracted and normalized to the intensity of the G band.

In addition to these Raman signals, the spectrum of nascent soot also presents a strong background due to photoluminescence emission. This latter contribution is commonly attributed to the organic fraction of the probed carbon matrix as also recently confirmed by thermo-optical transmission measurements combined to Raman spectroscopy analysis of several soot samples (Bocchicchio et al., 2022). Such results were also consistent with previously reported investigations, indicating a correlation of the photoluminescence background normalized to the intensity of the G band with the percentage of hydrogen in the carbon network (Casiraghi et al., 2005).

A deeper analysis of the photoluminescence emitted by the soot samples is obtained by the spectra recorded by the Raman

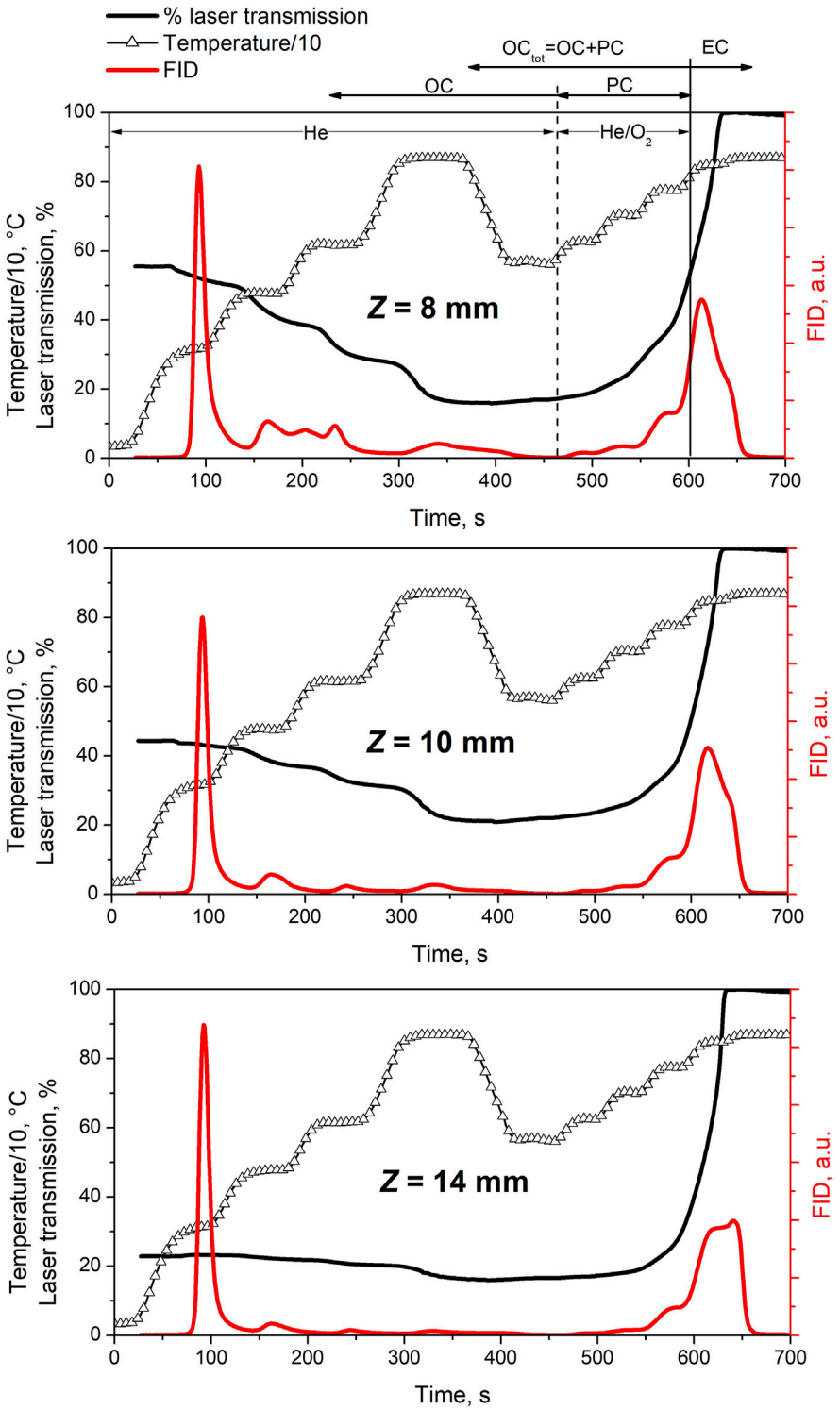

FIGURE 3 | Thermograms showing the adopted temperature program (line with triangles), the measured laser transmission (black line) and FID signal (red line) representative of carbonaceous material evolving off the quartz filter as a function of time. The vertical lines show the OC_{tot}/EC split (solid line), and the division between OC and "pyrolytically converted" OC, labeled PC (dashed line). Data refers to three soot samples at Z = 8 mm, Z = 10 mm and Z = 14 mm.

microscope over a wider spectral region. The spectra of the three samples are reported in **Figure 2A**. In order to compare the spectra of the three samples, the signals were divided by the Raman signal of Highly Ordered Pyrolytic Graphite (HOPG) as a reference material. As can be seen, the photoluminescence signal is very strong in samples collected at Z = 8 mm and Z = 10 mm, while it sensibly reduces in the sample collected at the higher height above the burner, i.e., Z = 14 mm. The integrated Raman G band of the samples Z8 and Z10 is about 15 times larger than the HOPG one. On the other hand, for the Z14 sample, i.e., the most mature soot in our study, the G band is only about 3 times larger, thus approaching the values reported by Le et al. (2017) for diesel soot. The larger Raman efficiency with respect to HOPG and the strong luminescence emission can indicate that the excitation wavelength is nearly resonant to an electronic transition of the particles and their structure is more similar to a molecular aggregate than a graphitic crystal. However, the increase of the Raman cross section in these structures can also be consequent to a larger number of vibrations that become Raman active with respect to pure graphite because of the relaxing of the selection rule based on the phonon momentum caused by the large number of defects. This effect causes the band linewidth and the integrated area to increase when moving form aged/mature soot to the just-nucleated incipient soot. In our samples, the linewidths of the G band are equal to 95, 83 and 68 cm^{-1} in the Z8, Z10 and Z14 samples, respectively and only to 10 cm^{-1} in HOPG. It is likely that in the investigated samples both effects occur, and so the signal intensity and the bandwidth are larger in the three soot samples compared to HOPG but they are also larger in Z10 and Z8 sample compared to Z14 sample. In light of all this, the just-nucleated particles can be considered like a disordered molecular solid that progressively transform towards a more graphitic compound by aging/maturation.

In order to better compare the lineshapes of the Raman signals, the Raman spectra have been baseline subtracted and normalized to the maximum of the G band. The Raman spectra of the three classes of nascent soot particles are reported in **Figure 2B**. The Raman D and G bands of the Z8 and Z10 samples present minor variations in their relative intensity, while the Z14 condition shows a slightly higher D band intensity that indicates a small increase of the in-plane size of the aromatic network composing the particles. Furthermore, the width and the other contributions to the first-order Raman spectrum present significant differences. Particularly, the inter-valley region between D and G peaks, as well as the signal in the spectral region 1700–2000 cm^{-1}, reduce as soot evolves in flame gradually changing from the Z8 to the Z14 samples. This is consistent to the increase of the graphitic order of the structure and reduction of the amorphous content.

Thermo-Optical Analysis

Figure 3 shows the thermograms for the three soot samples, namely Z8, Z10 and Z14. It can be noticed that the light transmittance of the filter decreases during the first, oxygen-free, heating phase. This indicates that PC carbon is formed. The amount of PC is evaluated measuring the carbon evolving from the filter from the beginning of the oxidative phase until the transmission reaches the original value. This point is denoted as split-time. Such interval is defined by the two vertical lines in **Figure 3A**: the dashed line indicates the starting of the oxidative phase and the solid line indicates the split-time.

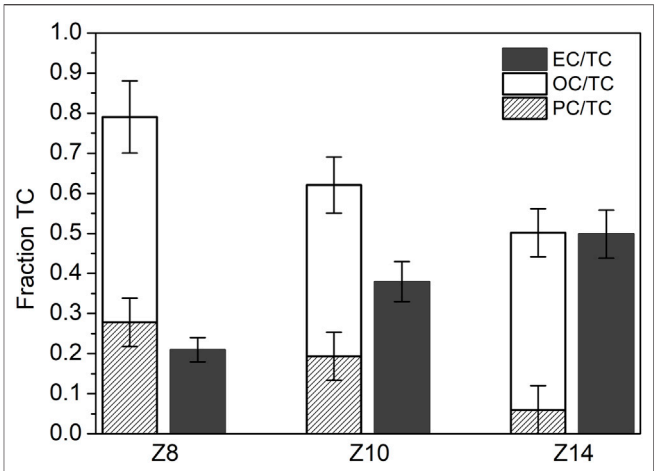

FIGURE 4 | Fractions of OC (Organic Carbon evolving in He), PC (Pyrolytic Carbon) and EC (Elemental Carbon) over the total carbon (TC) measured for each sample analyzed in this work, i.e., soot at Z = 8 mm, Z = 10 mm and Z = 14 mm.

After the calibration of the FID signal with a known amount of methane, the quantity of evolved carbon is evaluated by integrating the FID signal over the various peaks in the thermogram. **Figure 4** shows the three carbon contributions, i.e., OC, PC and EC, as fractions of the total mass of carbon (TC). As expected, the lowest amount of EC is measured in the Z8 sample consisting of only just-nucleated particles, while it becomes progressively larger in soot sampled upwards into the flame, i.e., Z10 and Z14, approaching the value of 50% of EC. Moreover, the trend of pyrolytic carbon shows that the percentage of PC fraction sensibly lowers moving from Z8 to the Z14 sample, while the OC fraction remains mostly constant over the three investigated samples.

The PC fraction is likely to be the major responsible for the photoluminescence emission excited by a laser beam in the visible at 532 nm. Indeed, the decrease of PC among the three samples has a similar evolution as the previously observed decrease of photoluminescence signal. The contribution to photoluminescence by the others two carbon fraction can be neglected. Indeed, the OC fraction that evolve from the filter in the He atmosphere is probably made of light molecules, loosely linked in the sample, that evolve from the filter instead of pyrolyzing when heated in an inert atmosphere. Conversely, the EC fraction is strongly absorbing visible light. However, the very low fluorescence in the sample H14, where EC fraction is the most abundant, indicates that the absorbed radiation is mainly dissipated through non radiative channel consistently with a graphitic-like component of the particle. The observed correlation between PC and luminescence

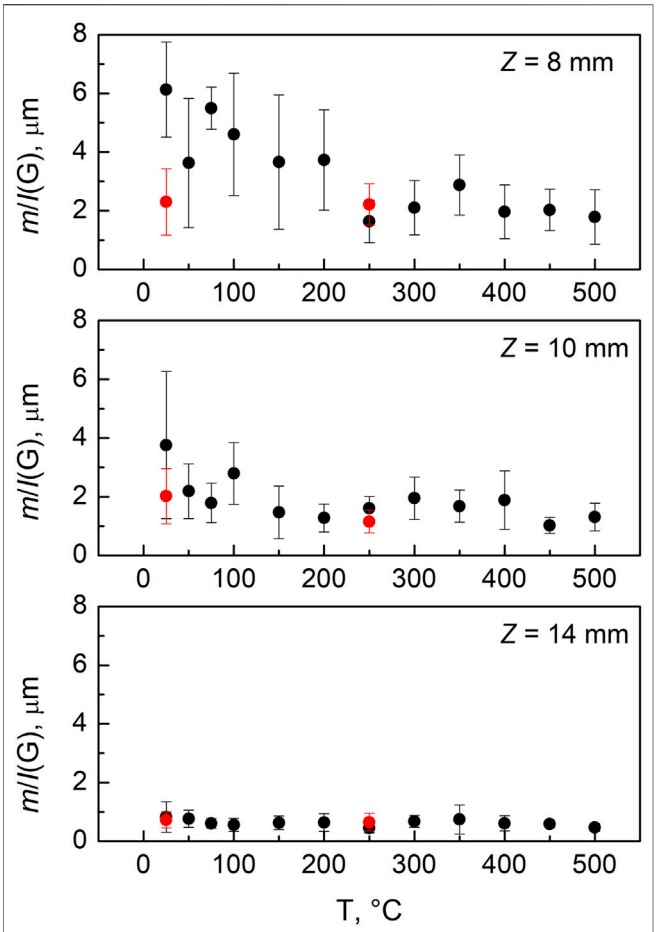

FIGURE 5 | *In situ* m/I(G) as a function of temperature for the three soot samples. The black dots refer to the heating stage; the red dots refer to the following cooling stage.

confirms the correlation reported in a previous work (Bocchicchio et al., 2022).

In-situ Raman Spectroscopy of Nascent Soot Oxidation

The three soot samples collected at different residence times have been exposed to a high temperature oxidation treatment in air up to 500°C. As a preliminary observation, we noticed that as temperature increased the contribution of the photoluminescence signal strongly reduces. This effect is reported in **Figure 5** as the ratio of the slope of the photoluminescence background, m, over the intensity of the G band, I(G). The m/I(G) ratio is commonly used within the carbon community as a parameter to follow the amount of hydrogen atoms in the carbon matrix (Casiraghi et al., 2005) and it has been recently correlated to the fraction of organic carbon content for similar soot particles (Bocchicchio et al., 2022). For the Z8 sample, this parameter reduces from a value of approximatively 6 µm to about 2 µm at high temperature. This indicates a reduction in the organic fraction of the sample due to the induced oxidation reactions. To a lower extent, a similar behavior can be observed for the Z10 condition, in this case m/I(G) decreases from ~4 µm to ~1.5 µm. The Z14 sample, which consists in a more mature soot particles with a very low photoluminescence signal, presents an almost invariance of the m/I(G) ratio. It is well known that an increase in temperature reduces both the fluorescence/photoluminescence lifetime and quantum efficiency of a fluorescing material favoring non-radiative quenching processes (Ossler et al., 2001). However, the effect we observe is not reversible and it is therefore due to a structural modification of the sample. This is demonstrated by the red dots in the **Figure 5**, showing the measurement obtained after the cooling process at room temperature. It is possible to observe that the signals do not return to the initial values, and this is a clear indication of the induced transformation/oxidation of the carbon material. A similar behavior was found by Ess et al. (2016) for soot with different organic carbon contents generated with a CAST burner at various propane-to-air ratios.

Figure 6 reports the Raman spectra of the three soot samples before and after the complete thermal-oxidative treatment, together with the spectral differences for each condition. For the Z8 sample, which is only composed by just-nucleated soot and has the highest amount of organic carbon fraction, the overall Raman spectrum of the post thermal/oxidative treatment sample presents a slight shift of the G band to lower wavenumbers, which is better seen from the derivative-like feature in the difference spectrum. This shift moves the G band towards the position of the G band in HOPG, i.e., 1,580 cm^{-1}, and probably indicates that, on average, the size of the aromatic clusters is increasing (Ferrari and Robertson, 2004), possibly caused by the removal of the smaller ones. Consistently, also a clear reduction of the other bands is evident, which are all activated by disorder. The decrease in the intensity is particularly evident for the spectral regions characteristic of the D4 band at ~ 1,200 cm^{-1}, the D band at ~ 1,350 cm^{-1} and the D3 band at ~1,500 cm^{-1}, following the terminology early adopted by Sadezky et al. (2005).

These bands are typically supposed to originate respectively from: polyenic chains attached to the edge of graphite crystallites and to small aromatic compounds (D4), the breathing of aromatic rings (D) and from amorphous carbon involving organic molecules, fragments, functional groups, and/or the inclusion of odd-membered ring structures that may also induce curvature or point defects in a graphitic lattice (D3). The lowering of all these components of the Raman spectrum due to the thermal oxidation process is, therefore, consistent with a preferential removal of the most organic and amorphous fraction of the carbon material composing the just-nucleated soot. This result is consistent with the earlier observations from Vander Wal and Tomasek (2004) by HRTEM on the strong dependence of soot reactivity from nanostructure. This finding is also consistent with the results recently obtained by Sediako et al. (2017) by *in-situ* oxidation HRTEM experiments showing that young soot was particularly prone to mass removal by oxidative reaction, owing to its low structural order. Similarly to the Z8 sample, the

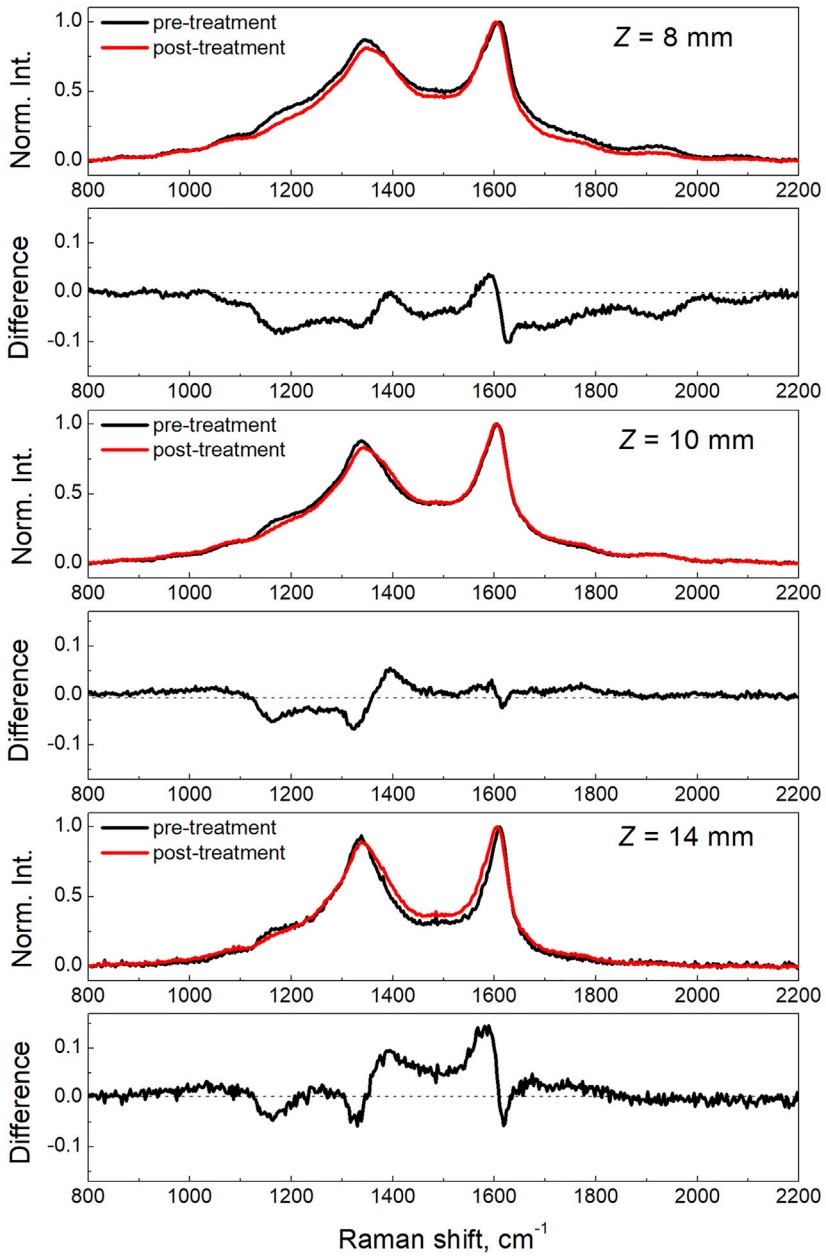

FIGURE 6 | Raman spectra of the three soot samples acquired at ambient temperature before and after the thermal/oxidation treatment performed up to a maximum temperature of 500°C.

intermediate case of Z10 shows a reduction of the D4 and D band intensity but a very little modification of the D3 band in the post oxidation Raman spectrum, as compared to the one of the pristine sample. Different is the case of the Z14 sample, particularly for the D3 band component that shows a sensible increase with respect to the pristine sample. The Z14 sample is composed by mature soot and carries about 50% of EC. The oxidation by O_2 may induce fragmentation or the formation of point defects in the graphitic component, thus increasing the amorphous character in the particles.

CONCLUSION

Three soot samples, characteristics of the early evolution of nascent soot in flames, have been collected from a lightly sooting ethylene/air laminar premixed flame by opportunely selecting the burner-to-probe distance, thus the particle residence time in the flame.

The pristine soot particles have been characterized in terms of organic and elemental carbon content by thermo-optical transmission measurements and in terms of structural

organization by Raman and photoluminescence spectroscopy. *In-situ* Raman spectroscopy has been used to probe carbon transformation of the three soot samples subject to early-stage oxidation process, over a range of temperature 25–500°C.

The three samples are: Z8, only comprising just-nucleated particles, i.e., those having an average diameter of approximatively 3 nm; Z14, made of mostly aged/mature soot; Z10, corresponding to an intermediate condition where both type of particles are present. The three samples contain the same fraction of OC, the organic fraction mostly made of light molecules evolving from the sample during heating in the inert atmosphere. The pyrolytic fraction, PC, decreases moving from Z8 to Z14 while the elemental carbon, EC, increases. The Raman and luminescence spectroscopies indicate that the just-nucleated particles can be considered like a disordered molecular solid that progressively transform towards a more graphitic compound by aging/maturation. This transformation seems to be mostly related to the PC fraction, i.e., the organic content prone to pyrolysis. The decrease of PC is indeed balanced by the increase of EC. Interestingly, the PC component decreases similarly to the photoluminescence (with the laser excitation wavelength in the visible region, i.e., λ = 532 nm).

The oxidation procedure mostly produced a strong reduction in the photoluminescence signal. Furthermore, the Raman spectroscopy shows that the sample with highest total organic content, i.e., Z8, after oxidation reduces the amorphous component. On the other hand, the Z14 condition (the sample with the highest content of EC) shows an increase in the amorphous phase that is attributed to fragmentation or the formation of point defects by O_2 oxidation.

DATA AVAILABILITY STATEMENT

The raw data supporting the conclusion of this article will be made available by the authors, without undue reservation.

AUTHOR CONTRIBUTIONS

GF designed the experiments, interpreted data and contributed to the writing of this manuscript. SB performed the experiments, collected and interpreted data. MC designed the experiments, collected and interpreted data and contributed to the writing of this manuscript. PM and AA designed experiments, interpreted data and contributed to the writing of this manuscript.

FUNDING

This work was financially supported by the United States Air Force Office of Scientific Research (AFOSR) under grant number FA8655-21-1-7022.

REFERENCES

Altarawneh, M., Oluwoye, I., and Dlugogorski, B. Z. (2020). Singlet-diradical Character in Large PAHs Triggers Spontaneous-Ignition of Coal Combust. *Combust. Flame* 212, 279–281. doi:10.1016/j.combustflame.2019.10.035

Apicella, B., Pré, P., Alfè, M., Ciajolo, A., Gargiulo, V., Russo, C., et al. (2015). Soot Nanostructure Evolution in Premixed Flames by High Resolution Electron Transmission Microscopy (HRTEM). *Proc. Combust. Inst.* 35, 1895–1902. doi:10.1016/j.proci.2014.06.121

Baldelli, A., Trivanovic, U., Sipkens, T. A., and Rogak, S. N. (2020). On Determining Soot Maturity: a Review of the Role of Microscopy-And Spectroscopy-Based Techniques. *Chemosphere* 252, 126532. doi:10.1016/j.chemosphere.2020.126532

Birch, M. E., and Cary, R. A. (1996). Elemental Carbon-Based Method for Monitoring Occupational Exposures to Particulate Diesel Exhaust. *Aerosol Sci. Technol.* 25, 221–241. doi:10.1080/02786829608965393

Bocchicchio, S., Commodo, M., Sgro, L. A., Chiari, M., D'Anna, A., and Minutolo, P. (2022). Thermo-optical-transmission OC/EC and Raman Spectroscopy Analyses of Flame-Generated Carbonaceous Nanoparticles. *Fuel* 310, 122308. doi:10.1016/j.fuel.2021.122308

Bond, T. C., Doherty, S. J., Fahey, D. W., Forster, P. M., Berntsen, T., DeAngelo, B. J., et al. (2013). Bounding the Role of Black Carbon in the Climate System: a Scientific Assessment. *J. Geophys. Res. Atmos.* 118, 5380–5552. doi:10.1002/jgrd.50171

Bonpua, J., Yagües, Y., Aleshin, A., Dasappa, S., and Camacho, J. (2019). Flame Temperature Effect on Sp^2 Bonds on Nascent Carbon Nanoparticles Formed in Premixed Flames ($T_{f,max}$ > 2100 K): A Raman Spectroscopy and Particle Mobility Sizing Study. *Proc. Combust. Inst.* 37, 943–951. doi:10.1016/j.proci.2018.06.124

Botero, M. L., Sheng, Y., Akroyd, J., Martin, J., Dreyer, J. A. H., Yang, W., et al. (2019). Internal Structure of Soot Particles in a Diffusion Flame. *Carbon* 141, 635–642. doi:10.1016/j.carbon.2018.09.063

Cain, J. P., Camacho, J., Phares, D. J., Wang, H., and Laskin, A. (2011). Evidence of Aliphatics in Nascent Soot Particles in Premixed Ethylene Flames. *Proc. Combust. Inst.* 33, 533–540. doi:10.1016/j.proci.2010.06.164

Camacho, J., Tao, Y., and Wang, H. (2015). Kinetics of Nascent Soot Oxidation by Molecular Oxygen in a Flow Reactor. *Proc. Combust. Inst.* 35, 1887–1894. doi:10.1016/j.proci.2014.05.095

Casiraghi, C., Piazza, F., Ferrari, A. C., Grambole, D., and Robertson, J. (2005). Raman Spectroscopy of Hydrogenated Amorphous Carbons. *Diam. Relat. Mater.* 14, 1098–1102. doi:10.1016/j.diamond.2004.10.030

Castiglioni, C., Negri, F., Rigolio, M., and Zerbi, G. (2001). Raman Activation in Disordered Graphites of the A′1 Symmetry Forbidden K≠0 Phonon: The Origin of the D Line. *J. Chem. Phys.* 115, 3769–3778. doi:10.1063/1.1381529

Chow, J. C., Watson, J. G., Chen, L.-W. A., Arnott, W. P., Moosmüller, H., and Fung, K. (2004). Equivalence of Elemental Carbon by Thermal/optical Reflectance and Transmittance with Different Temperature Protocols. *Environ. Sci. Technol.* 38, 4414–4422. doi:10.1021/es034936u

Commodo, M., De Falco, G., Bruno, A., Borriello, C., Minutolo, P., and D'Anna, A. (2015). Physicochemical Evolution of Nascent Soot Particles in a Laminar Premixed Flame: from Nucleation to Early Growth. *Combust. Flame* 162, 3854–3863. doi:10.1016/j.combustflame.2015.07.022

Commodo, M., Kaiser, K., De Falco, G., Minutolo, P., Schulz, F., D'Anna, A., et al. (2019). On the Early Stages of Soot Formation: Molecular Structure Elucidation by High-Resolution Atomic Force Microscopy. *Combust. Flame* 205, 154–164. doi:10.1016/j.combustflame.2019.03.042

Commodo, M., Karataş, A. E., De Falco, G., Minutolo, P., D'Anna, A., and Gülder, Ö. L. (2020). On the Effect of Pressure on Soot Nanostructure: A Raman Spectroscopy Investigation. *Combust. Flame* 219, 13–19. doi:10.1016/j.combustflame.2020.04.008

Davidson, C. I., Phalen, R. F., and Solomon, P. A. (2005). Airborne Particulate Matter and Human Health: A Review. *Aerosol Sci. Technol.* 39, 737–749. doi:10.1080/02786820500191348

De Falco, G., Mattiello, G., Commodo, M., Minutolo, P., Shi, X., D'Anna, A., et al. (2021). Electronic Band Gap of Flame-Formed Carbon Nanoparticles by Scanning Tunneling Spectroscopy. *Proc. Combust. Inst.* 38, 1805–1812. doi:10.1016/j.proci.2020.07.109

De Falco, G., Picca, F., Commodo, M., and Minutolo, P. (2020). Probing Soot Structure and Electronic Properties by Optical Spectroscopy. *Fuel* 259, 116244. doi:10.1016/j.fuel.2019.116244

Decesari, S., Facchini, M. C., Matta, E., Mircea, M., Fuzzi, S., Chughtai, A. R., et al. (2002). Water Soluble Organic Compounds Formed by Oxidation of Soot. *Atmos. Environ.* 36, 1827–1832. doi:10.1016/s1352-2310(02)00141-3

Echavarria, C. A., Jaramillo, I. C., Sarofim, A. F., and Lighty, J. S. (2012). Burnout of Soot Particles in a Two-Stage Burner with a JP-8 Surrogate Fuel. *Combust. Flame* 159, 2441–2448. doi:10.1016/j.combustflame.2012.03.011

Echavarria, C. A., Jaramillo, I. C., Sarofim, A. F., and Lighty, J. S. (2011). Studies of Soot Oxidation and Fragmentation in a Two-Stage Burner under Fuel-Lean and Fuel-Rich Conditions. *Proc. Combust. Inst.* 33, 659–666. doi:10.1016/j.proci.2010.06.149

Ess, M. N., Ferry, D., Kireeva, E. D., Niessner, R., Ouf, F.-X., and Ivleva, N. P. (2016). *In Situ* Raman Microspectroscopic Analysis of Soot Samples with Different Organic Carbon Content: Structural Changes during Heating. *Carbon* 105, 572–585. doi:10.1016/j.carbon.2016.04.056

Faccinetto, A., Irimiea, C., Minutolo, P., Commodo, M., D'Anna, A., Nuns, N., et al. (2020). Evidence on the Formation of Dimers of Polycyclic Aromatic Hydrocarbons in a Laminar Diffusion Flame. *Commun. Chem.* 3 (1). art. no. 112, 1–8. doi:10.1038/s42004-020-00357-2

Ferrari, A. C., and Robertson, J. (2004). Raman Spectroscopy of Amorphous, Nanostructured, Diamond-like Carbon, and Nanodiamond. *Philosophical Trans. R. Soc. Lond. Ser. A Math. Phys. Eng. Sci.* 362, 2477–2512. doi:10.1098/rsta.2004.1452

Ghiassi, H., Jaramillo, I. C., Toth, P., and Lighty, J. S. (2016a). Soot Oxidation-Induced Fragmentation: Part 2: Experimental Investigation of the Mechanism of Fragmentation. *Combust. FlameFlame* 163, 170–178. doi:10.1016/j.combustflame.2015.09.022

Ghiassi, H., Toth, P., Jaramillo, I. C., and Lighty, J. S. (2016b). Soot Oxidation-Induced Fragmentation: Part 1: The Relationship between Soot Nanostructure and Oxidation-Induced Fragmentation. *Combust. Flame* 163, 179–187. doi:10.1016/j.combustflame.2015.09.023

Giannoni, M., Calzolai, G., Chiari, M., Cincinelli, A., Lucarelli, F., Martellini, T., et al. (2016). A Comparison between Thermal-Optical Transmittance Elemental Carbon Measured by Different Protocols in $PM_{2.5}$ Samples. *Sci. Total Environ.* 571, 195–205. doi:10.1016/j.scitotenv.2016.07.128

Hansen, J., and Nazarenko, L. (2004). Soot Climate Forcing via Snow and Ice Albedos. *Proc. Natl. Acad. Sci. U.S.A.* 101, 423–428. doi:10.1073/pnas.2237157100

Herdman, J. D., Connelly, B. C., Smooke, M. D., Long, M. B., and Miller, J. H. (2011). A Comparison of Raman Signatures and Laser-Induced Incandescence with Direct Numerical Simulation of Soot Growth in Non-premixed Ethylene/air Flames. *Carbon* 49, 5298–5311. doi:10.1016/j.carbon.2011.07.050

Kennedy, I. M. (2007). The Health Effects of Combustion-Generated Aerosols. *Proc. Combust. Inst.* 31, 2757–2770. doi:10.1016/j.proci.2006.08.116

Kholghy, M., Saffaripour, M., Yip, C., and Thomson, M. J. (2013). The Evolution of Soot Morphology in a Laminar Coflow Diffusion Flame of a Surrogate for Jet A-1. *Combust. Flame* 160, 2119–2130. doi:10.1016/j.combustflame.2013.04.008

Le, K. C., Lefumeux, C., and Pino, T. (2017). Differential Raman Backscattering Cross Sections of Black Carbon Nanoparticles. *Sci. Rep.* 7, 17124. doi:10.1038/s41598-017-17300-6

Martin, J. W., Salamanca, M., and Kraft, M. (2022). Soot Inception: Carbonaceous Nanoparticle Formation in Flames. *Prog. Energy Combust. Sci.* 88, 100956. doi:10.1016/j.pecs.2021.100956

Michelsen, H. A., Colket, M. B., Bengtsson, P.-E., D'Anna, A., Desgroux, P., Haynes, B. S., et al. (2020). A Review of Terminology Used to Describe Soot Formation and Evolution under Combustion and Pyrolytic Conditions. *ACS Nano* 14, 12470–12490. doi:10.1021/acsnano.0c06226

Minutolo, P., Commodo, M., Santamaria, A., De Falco, G., and D'Anna, A. (2014). Characterization of Flame-Generated 2-D Carbon Nano-Disks. *Carbon* 68, 138–148. doi:10.1016/j.carbon.2013.10.073

Minutolo, P., Rusciano, G., Sgro, L. A., Pesce, G., Sasso, A., and D'Anna, A. (2011). Surface Enhanced Raman Spectroscopy (SERS) of Particles Produced in Premixed Flame across Soot Threshold. *Proc. Combust. Inst.* 33, 649–657. doi:10.1016/j.proci.2010.07.077

Molina, M. J., Ivanov, A. V., Trakhtenberg, S., and Molina, L. T. (2004). Atmospheric Evolution of Organic Aerosol. *Geophys. Res. Lett.* 31, L22104. doi:10.1029/2004gl020910

Nagle, J., and Strickland-Constable, R. F. (1962). "Oxidation of Carbon between 1000-2000°C," in Proceedings of the Fifth Conference on Carbon, 154–164. doi:10.1016/b978-0-08-009707-7.50026-1

Niessner, R. (2014). The Many Faces of Soot: Characterization of Soot Nanoparticles Produced by Engines. *Angew. Chem. Int. Ed. Engl.* 53, 12366–12379. doi:10.1002/anie.201402812

Nobili, A., Pratali Maffei, L., Baggioli, A., Pelucchi, M., Cuoci, A., Cavallotti, C., et al. (2022). On the Radical Behavior of Large Polycyclic Aromatic Hydrocarbons in Soot Formation and Oxidation. *Combust. Flame* 235, 111692. doi:10.1016/j.combustflame.2021.111692

Ossler, F., Metz, T., and Aldén, M. (2001). Picosecond Laser-Induced Fluorescence from Gas-phase Polycyclic Aromatic Hydrocarbons at Elevated Temperatures. I. Cell Measurements. *Appl. Phys. B* 72, 465–478. doi:10.1007/s003400100519

Pedata, P., Stoeger, T., Zimmermann, R., Peters, A., Oberdörster, G., and D'Anna, A. (2015). "Are We Forgetting the Smallest, Sub 10 Nm Combustion Generated Particles?". *Part Fibre Toxicol.* 12, 34. doi:10.1186/s12989-015-0107-3

Sadezky, A., Muckenhuber, H., Grothe, H., Niessner, R., and Pöschl, U. (2005). Raman Microspectroscopy of Soot and Related Carbonaceous Materials: Spectral Analysis and Structural Information. *Carbon* 43, 1731–1742. doi:10.1016/j.carbon.2005.02.018

Salamanca, M., Botero, M. L., Martin, J. W., Dreyer, J. A. H., Akroyd, J., and Kraft, M. (2020). The Impact of Cyclic Fuels on the Formation and Structure of Soot. *Combust. Flame* 219, 1–12. doi:10.1016/j.combustflame.2020.04.026

Santamaría, A., Mondragón, F., Molina, A., Marsh, N. D., Eddings, E. G., and Sarofim, A. F. (2006). FT-IR and 1H NMR Characterization of the Products of an Ethylene Inverse Diffusion Flame. *Combust. Flame* 146, 52–62. doi:10.1016/j.combustflame.2006.04.008

Schulz, F., Commodo, M., Kaiser, K., De Falco, G., Minutolo, P., Meyer, G., et al. (2019). Insights into Incipient Soot Formation by Atomic Force Microscopy. *Proc. Combust. Inst.* 37, 885–892. doi:10.1016/j.proci.2018.06.100

Sediako, A. D., Soong, C., Howe, J. Y., Kholghy, M. R., and Thomson, M. J. (2017). Real-time Observation of Soot Aggregate Oxidation in an Environmental Transmission Electron Microscope. *Proc. Combust. Inst.* 36, 841–851. doi:10.1016/j.proci.2016.07.048

Seong, H. J., and Boehman, A. L. (2013). Evaluation of Raman Parameters Using Visible Raman Microscopy for Soot Oxidative Reactivity. *Energy fuels.* 27, 1613–1624. doi:10.1021/ef301520y

Sirignano, M., Ghiassi, H., D'Anna, A., and Lighty, J. S. (2016). Temperature and Oxygen Effects on Oxidation-Induced Fragmentation of Soot Particles. *Combust. Flame* 171, 15–26. doi:10.1016/j.combustflame.2016.05.011

Sirignano, M., Kent, J., and D'Anna, A. (2013). Modeling Formation and Oxidation of Soot in Nonpremixed Flames. *Energy fuels.* 27, 2303–2315. doi:10.1021/ef400057r

Vander Wal, R. L., and Tomasek, A. J. (2004). Soot Nanostructure: Dependence upon Synthesis Conditions. *Combust. Flame* 136, 129–140. doi:10.1016/j.combustflame.2003.09.008

Vitiello, G., De Falco, G., Picca, F., Commodo, M., D'Errico, G., Minutolo, P., et al. (2019). Role of Radicals in Carbon Clustering and Soot Inception: A Combined EPR and Raman Spectroscopic Study. *Combust. Flame* 205, 286–294. doi:10.1016/j.combustflame.2019.04.028

Yu, J. Z., Xu, J., and Yang, H. (2002). Charring Characteristics of Atmospheric Organic Particulate Matter in Thermal Analysis. *Environ. Sci. Technol.* 36, 754–761. doi:10.1021/es015540q

Zhang, H.-B., You, X., and Law, C. K. (2015). Role of Spin-Triplet Polycyclic Aromatic Hydrocarbons in Soot Surface Growth. *J. Phys. Chem. Lett.* 6 (3), 477–481. doi:10.1021/jz502635t

Zuberi, B., Johnson, K. S., Aleks, G. K., Molina, L. T., Molina, M. J., and Laskin, A. (2005). Hydrophilic Properties of Aged Soot. *Geophys. Res. Lett.* 32, 1–4. doi:10.1029/2004gl021496

Conflict of Interest: The authors declare that the research was conducted in the absence of any commercial or financial relationships that could be construed as a potential conflict of interest.